



**HAL**  
open science

## Brillouin mirror with inverted acoustic profile in presence of strong acoustic dispersion

Antonio Montes, Carlos Montes, Éric Picholle

► **To cite this version:**

Antonio Montes, Carlos Montes, Éric Picholle. Brillouin mirror with inverted acoustic profile in presence of strong acoustic dispersion. *Journal of the Optical Society of America B*, 2021, 38 (2), pp.456-465. hal-02906584

**HAL Id: hal-02906584**

**<https://hal.science/hal-02906584>**

Submitted on 25 Jul 2020

**HAL** is a multi-disciplinary open access archive for the deposit and dissemination of scientific research documents, whether they are published or not. The documents may come from teaching and research institutions in France or abroad, or from public or private research centers.

L'archive ouverte pluridisciplinaire **HAL**, est destinée au dépôt et à la diffusion de documents scientifiques de niveau recherche, publiés ou non, émanant des établissements d'enseignement et de recherche français ou étrangers, des laboratoires publics ou privés.



Distributed under a Creative Commons Attribution - NonCommercial - NoDerivatives 4.0 International License

# Brillouin mirror with inverted acoustic profile in presence of strong acoustic dispersion

ANTONIO MONTES,<sup>1</sup> CARLOS MONTES,<sup>2</sup> AND ÉRIC PICHOLLE<sup>2,\*</sup>

<sup>1</sup>*Department of Applied Mathematics II (MA2), Universitat Politècnica de Catalunya, Barcelone, Spain*

<sup>2</sup>*Institut de Physique de Nice (INPHYNI), UMR 7010 Université Côte d'Azur & CNRS, Parc Valrose, 06108 Nice cedex, France*

\*[eric.picholle@inphyni.cnrs.fr](mailto:eric.picholle@inphyni.cnrs.fr)

**Abstract:** While usually negligible in standard optical fibers, the group velocity dispersion of acoustic waves may in some cases play a significant role in the dynamics of stimulated Brillouin scattering (SBS) in propagation medias with more complex structures, such as microstructured fibers. The usual 3-wave coherent model of SBS can be adapted to take a perturbative acoustic dispersion into account, but the slowly varying envelopes approximation does not hold for stronger values of the acoustic dispersion, which call for a more sophisticated inertial model of SBS. A new regime of SBS mirror with a spatially inverted acoustic profile is predicted in this limit. In presence of strong acoustic dispersion, this regime exhibits a higher conversion efficiency than the usual mirror in the dispersionless case, as well as nonlinear self-stabilization of the phase of the acoustic wave when the pump is strongly depleted. Formal calculations allow the identification of regions of strong dynamic dispersion.

## 1. Introduction

Stimulated Brillouin scattering (SBS) could once appear as a very well understood nonlinear phenomenon in optical fibers and waveguides, with a robust coherent three-wave model [1, 2] fully accounting for its extremely rich dynamics in 1D-media such as single-mode silica optical fibers (SMF). Indeed, besides the common 'SBS mirror' [3, 4], both self-stabilized ultracoherent regimes [5–8], bifurcations [9] and bistability [10], soliton regimes [6, 11], SBS chaos [12, 13] and even SBS rogue waves [14, 15] in SMFs are well described by this 3-wave model.

Nevertheless, a kind of 'renaissance in Brillouin scattering research' could recently be heralded [16], with a remarkable extension of the realm of Brillouin lasers in numerous and varied new kinds of waveguides, including microstructured fibers, silica [17] or chalcogenide [18], but also multicore fibers [19], micro- and nano-fibers [20, 21], hollow core PCFs [22, 23] as well as silicon [24] and silicon nitride [25, 26] waveguides, optomechanical waveguides [27] and even on-chip SBS laser devices [28].

In particular, the growing technological importance of photonic crystal fibers (PCF) yielded special interest on the acoustical properties of small-core PCFs, which microstructuring substantially changes the acoustic dispersion relation, and even the general acoustic properties [29–32] compared to conventional single-mode fibers.

Recent advances in cavity optomechanics also allowed to design tight confinement structures with acoustic dispersion values that deviate substantially from the usual linear dispersion relation of bulk materials or traditional SMFs [33], or even nontrivial topological acoustic band structures at interfaces [34]. A direct corollary is that some tightly confined acoustic modes may present a finite cutoff frequency, yielding a flat, Raman-like acoustic dispersion relation  $\omega_a(k_a)$  [19, 25, 29], that is, a strong acoustic group velocity dispersion near cutoff.

The aim of this article is to explore the consequences of the acoustic dispersion on the 1D dynamics of SBS. After showing that even perturbative values of this dispersion, still compatible with an adaptation the usual 3-wave model (§3), can in some cases induce quite significant effects, we will consider the consequences of a stronger acoustic dispersion. We show that, relaxing the slowly varying envelopes (SVE) approximation, a new SBS mirror regime with an

inverted acoustic profile and a low threshold can be predicted through a more complete inertial 3-wave model of SBS, and we discuss its specific features (§4). Finally, we will identify potential regions of strong dynamic acoustic dispersion (§5). An Appendix considers the quite complicated acoustic dispersion relation in the inertial limit.

## 2. Dispersionless case

### 2.1. Standard coherent 3-wave model of SBS

The now standard 3-wave model for SBS optical fibers [1, 2, 35, 36] and, more recently, for some optomechanical cavities [37] was originally derived from the coherent model of SBS in laser-plasma interactions [38–41]. It is usually assumed that the slowly varying envelopes approximation holds for both optical waves (pump and Brillouin, of respective frequencies  $\omega_p$  and  $\omega_B$ ), as well as for the acoustic wave, of frequency  $\omega_a$ , as long as nanosecond or longer pulsed regimes, or *a fortiori* stationary or quasi-stationary regimes, are considered. In the 1D (or quasi-1D) approximation, the coupled evolution equations for the pump ( $E_p$ ), backscattered Brillouin ( $E_B$ ), and acoustic ( $E_a$ ) complex amplitudes read :

$$(\partial_t + c/n \partial_x + \gamma_e) E_p = -K_{SBS} E_B E_a \quad (1)$$

$$(\partial_t - c/n \partial_x + \gamma_e) E_B = K_{SBS} E_p E_a^* \quad (2)$$

$$(\partial_t + c_a \partial_x + \gamma_a) E_a = K_{SBS} E_p E_B^* \quad (3)$$

where the material density  $\rho$  is dimensioned to an equivalent electric field through  $\rho = i\sigma E_a$ , with  $\sigma^2 = \frac{\rho_0 n^3 \epsilon_0}{2cc_a}$ ,  $\gamma_e$  and  $\gamma_a$  are the optical and acoustical losses coefficients, respectively,  $n$  is the effective optical index (usually considered identical at both pump and Brillouin frequencies for numerical simulations, but distinct values can easily be taken into account) and  $c_a$  the effective phase velocity of the considered acoustic mode.

$K_{SBS} = \sqrt{\frac{\epsilon_0 n^7 p_{12}^2}{8\rho_0 c_a c}} \omega_p$  is the SBS coupling coefficient, with  $p_{12}$  the effective elasto-optic coefficient of the material [1]. Additional terms in Eq. (3) can account for the initiation of SBS from thermal noise [2], and in Eqs. (1 & 2) for a perturbative optical Kerr effect [1].

Let us emphasize that, since SBS is a coherent 3-wave process, the energy transfers can happen both ways (i.e. Stokes process : creation of a Brillouin photon and an acoustic phonon at the expense of a pump photon; antiStokes : creation of a pump photon by recombination of a Brillouin photon and an acoustic phonon), depending on the relative phases of the three waves. More precisely, the gain is locally proportional to  $\cos \Phi$ , where  $\Phi = \varphi_p - \varphi_B - \varphi_a$ , and  $\varphi_{p,B,a}$  are respectively the phases of the pump, Brillouin and acoustic waves.

The acoustic propagation term in Eq. (3) is often neglected for simplicity, at the cost of superimposing an arbitrary gain linewidth that otherwise can be directly derived from system (1-3) in the stationary regime [42, 43].

The 1D approximation generally holds regardless of the polarization of the acoustic mode as long as only one such mode at the time is considered [44], typically in SBS lasers or amplifiers. Few-mode operation, either optical or acoustical, can still be taken into account in a quasi-1D approach by introducing additional coupled equations, allowing for instance to describe the coupling between longitudinal and radial or torso-radial acoustic modes in SMFs [45–47] or in hollow-core PCFs [22]. Nevertheless, the situation becomes intrinsically 3D when a continuum of bulk elastic waves must be considered [44].

## 2.2. Common SBS mirror

In the full (phases as well as amplitudes) stationary approximation, the 3-wave coherent model can be reduced to a 2-wave (pump & Brillouin) 'intensity model' by re-injecting  $E_a = E_p E_B^* / \gamma_a$  into Eqs. (1 & 2), whose long-known stationary solution [3,4] is known as a 'SBS mirror' [35,36,42].

In this regime, the intensities of the three waves ( $I_{p,B,a}(x) = |E_{p,B,a}(x)|^2$ ) monotonously decrease from their maximum value at the fiber end closest to the pump laser (left in Fig. 1). When the optical losses can be neglected, the counterpropagating pump and Brillouin waves are parallel ( $I_p(x) - I_B(x) = Cst$ ), the slave acoustic wave  $I_a(x) \propto I_p(x)I_B(x)$  following a similar distribution (Fig. 1).

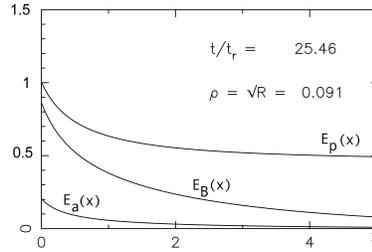


Fig. 1. Common (dispersionless,  $\alpha = 0$ ) SBS mirror: Spatial distribution of the amplitudes of the three waves (numerical, the dimensionless abscissa is the reduced fiber length  $x \rightarrow x/\Lambda = nK_{SBS}\sqrt{I_p^0}x/c$ ;  $G = 14.5$ ;  $L/\Lambda = 30$ ,  $\mu = 4.24$ ,  $\sqrt{R} = 0.091$ ,  $t/t_r = 25.46$ ). Note that the intensities of *all three* waves monotonously decrease from the laser input end (left).

Further neglecting the pump depletion would yield an exponential amplification of the Brillouin wave :  $I_B(x) = I_B^L e^{g_{SBS} I_p^0 (L-x)}$  where  $g_{SBS} = \frac{nK_{SBS}^2}{c\gamma_a}$  is the SBS gain.  $G = g_{SBS} I_p^0 L$  is also a useful dimensionless gain parameter [1].

Nevertheless, the intensity model cannot describe the coherent properties of SBS, such as the finite width of the gain profile centered around the resonant SBS frequency  $\omega_B^{res}$  defined by the phase-matching conditions  $\mathbf{k}_p = \mathbf{k}_B^{res} + \mathbf{k}_a^{res}$  and  $\omega_p = \omega_B^{res} + \omega_a^{res}$ , where  $k_p = n\omega_p/c$ ,  $k_B^{res} = n\omega_B^{res}/c$  and  $k_a^{res} = \omega_a^{res}/c_a$ .

When the stationary phase approximation is relaxed to allow off-resonance interaction [42,43], the coherent 3-wave model yields in the single-frequency seeded SBS amplifier configuration the traditional lorentzian gain profile of width (FWHM)  $\gamma_a$ .

When the SBS amplification starts from the acoustic noise [2], the reflectivity  $I_B^0/I_p^0$  of the mirror becomes significant for large enough gains (typically,  $G > 21$  in standard SMFs [35]), depending also on the fiber modal structure and strain distribution [48]. In a SBS laser, the efficiency of the common SBS mirror is determined by the boundary conditions, the output Brillouin intensity being usually higher than the input pump intensity. Typically, the common SBS mirror shown in Fig. 1 presents a reflectivity of 75% for a gain  $G = 14.5$ .

## 3. SBS in presence of weak acoustic dispersion

### 3.1. 3-wave model with perturbative acoustic dispersion

While the issue of the acoustic group velocity dispersion in fibers is a well-known problem in guided acoustics [49,50], including in the context of SBS in microstructured fibers where specific

losses may strongly affect the acoustic dispersion relation [31, 51], it has mostly been applied to specific metrology applications [52].

In order to consider its influence on the SBS dynamics, a first approach is to adapt the coherent 3-wave model by integrating in the acoustic Eq. (3) an additional perturbative term  $i\beta_a \partial_{tt}$ , where  $\beta_a = c_a \frac{d^2 k_a}{d\omega_a^2} \ll 1$  is the acoustic group velocity dispersion coefficient, yielding:

$$(\partial_t + c_a \partial_x + i\beta_a \partial_{tt} + \gamma_a) E_a = K_{SBS} E_p E_B^* \quad (4)$$

### 3.2. Stationary SBS mirror

In the full stationary approximation,  $\partial_{tt} E_a = 0$  and the SBS mirror solution [3, 4] is obviously identical for both models with [Eqs. (1, 2 & 3)] and without [Eqs. (1, 2 & 4)] acoustic dispersion. The SBS gain remains unchanged. Taking into account both first order optical and acoustical dispersion yields a somewhat more complicated form of the gain profile of SBS amplifiers when the intensities are constant but not the phases, with:

$$g_{SBS}(\Omega) = \frac{\gamma_a^2}{\gamma_a^2 + [(k'_a + k'_e) \Omega]^2} g_{SBS}^{res} \quad (5)$$

where  $g_{SBS}^{res}$  is the usual SBS gain at resonance;  $\Omega = \omega_B - \omega_B^{res} = \omega_a^{res} - \omega_a$ ;  $k'_a c_a^{res} = 1 - \omega_a^{res} \frac{\partial c_a}{\partial \omega_a} |_{\omega_a^{res}}$ ; and  $k'_e c = n + \omega_B^{res} \frac{\partial n}{\partial \omega_B} |_{\omega_B^{res}}$ .

It is interesting to note that the maximum value of the gain, at resonance, is not modified, but that this expression predicts an almost flat SBS gain whenever  $(k'_a + k'_e) = 0$ , i.e.  $\lambda_B \approx \frac{c_a}{2\pi} (\frac{\partial n}{\partial \omega_B} - 2n \frac{\partial c_a}{\partial \omega_a})$ .

### 3.3. Dynamics of SBS solitons in presence of weak acoustic dispersion

Like single-mode fiber SBS lasers [6], PCF lasers with small enough feedback [9] exhibit pulsed solitonic behaviours. Our reference will be the experiment by Woodward et al. [17], where a SBS linear cavity is constituted by the small Fresnel reflexions at both ends of a 9m-long PCF fiber with a  $3\mu\text{m}$  core and an hexagonal structure of  $0.7\mu\text{m}$  air holes spaced by  $1.9\mu\text{m}$ , yielding an effective area of  $4.73\mu\text{m}^2$  at the pump wavelength  $\lambda_p = 532\text{nm}$ . For pump powers between 57 and 123mW, they observed stable solitonic outputs, either sub- or superluminal, with pulses widths (FWHM) of  $14.5\text{nsec} \pm 1.5\text{nsec}$  [53]. This 10% fluctuation in soliton width could not be simply interpreted in the frame of the dispersionless 3-wave model.

Although neither the acoustic dispersion of the PCF fiber used in this experiment, nor *a fortiori* its dependence on the pump wavelength, has been determined, a possible interpretation of this fluctuation would make it a consequence of a steep dispersion relation of the involved acoustic mode.

Thus, we performed numerical simulations of the Woodward experiment through the 3-wave model both without [Eqs. (1,2 & 3),  $\beta_a = 0$ ] and with [Eqs. (1,2 & 4),  $\beta_a = 0.01$ ] perturbative acoustic dispersion. The normalized SBS gain was set at  $G = 10.5$ , corresponding to an injected pump power  $I_p$  of about 100mW, and the small (intensity) reinjection coefficient  $\sqrt{R} = 0.091$ , ensuring a dynamics well into the solitonic region [10].

As expected, both simulations yielded stable solitonic outputs (Fig. 2), in sound qualitative agreement with the experiment, but with quite different quantitative features. Indeed, all other parameters being identical, the dispersionless model yielded almost luminal ( $v_{signal} = 1.005 c/n$ ) with a width (FWHM) around 5 nsec, or 0.125 linear roundtrip time [Fig. 2, left], while  $\beta_a = 0.01$  yielded slightly faster ( $v_{signal} = 1.025 c/n$ ), but significantly compressed pulses, with a width of 4.6 nsec [Fig. 2, right], or a compression factor of 15 %. These value roughly corresponded to the extreme experimental values for the largest and slowest, and most narrow and fastest observed pulses, respectively.

A perturbative acoustic dispersion value thus appears sufficient to induce significant changes in the dynamics of a SBS laser, allowing typically for the possibility of a 10 to 15% variations in the SBS solitons temporal width, and a 2% velocity variation in such devices for  $\beta_a$  variations of the order of 1% from run to run, depending for instance on the exact pump wavelength or even on room temperature fluctuations.

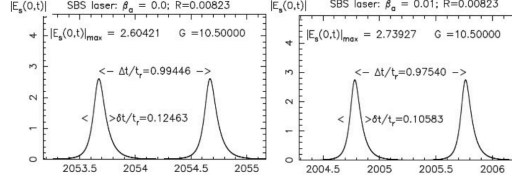


Fig. 2. Output of a soliton laser (numerical, coherent 3-wave SVE model for a gain  $G = 10.5$ ,  $\sqrt{R} = 0.091$ ). Left: Amplitude  $E_B(0, t)$  of the Brillouin output without dispersion ( $\beta_a = 0$ ), the soliton travel at almost luminal velocity ( $v = 1.005 c/n$ ); right: *idem*, but taking into account a perturbative acoustic dispersion ( $\beta_a = 0.01$ ), the velocity slightly increases ( $v = 1.026 c/n$ ) while the solitons are compressed by about 15%. (numerical. The parameters correspond to those of the experiment described in [17].)

## 4. Inertial model of SBS in presence of strong acoustic dispersion

### 4.1. Inertial model

A key feature of the acoustic wave produced through the stimulated Brillouin process is its long lifetime, typically in the 10 ns range, well above the duration of the optical pulses used in telecommunications, yielding for instance long range interaction between the latter in fiber telecommunications [54,55]. A soliton train is best described by a standard nonlinear Schrödinger (NLS) equation whose solutions are injected as source input in Eq. (1) [56].

A similar procedure can be followed to take into account a strong acoustic group velocity dispersion. When the slowly varying envelopes approximation is dropped, the acoustic dispersion relation may become quite complicated (see Appendix), like in the strong field limit previously explored in laser-plasma SBS interactions [57]. We may thus write  $\beta_a = \beta_a^{mat} + \beta_a^{inert}$ , where  $\beta_a^{inert}$  is the inertial part of the acoustic dispersion, which can become dominant for rapidly evolving acoustic fields.

We thus define the generalized acoustic dispersion parameter  $\alpha = c_a \frac{d^2 k_a}{d\omega_a^2}(\omega_a) K_{SBS} \sqrt{I_p^0} / 2\omega_a$ . Note than, even when the inertial part of the dispersion can be neglected, the reduced parameter  $\alpha$  may cease to be perturbative not only for very high values of the material acoustic GVD  $\beta_a^{mat}$ , but also, for a given  $\beta_a^{mat}$ , for high input pump intensities.

To obtain the so-called 'inertial' model of SBS [57], we can now re-write Eq. (1) for non-slowly varying *acoustic* envelopes, yielding:

$$[(1 + 2i\alpha)\partial_t + c_a\partial_x + i\alpha(\partial_{tt} - \varepsilon^2\partial_{xx} + \gamma_a)] E_a = K_{SBS} E_p E_B^* \quad (6)$$

where the small parameter  $\varepsilon = c_a/c$  is of the order of  $10^{-5}$ .

Substituting again the full Eq. (6) to the perturbative Eq. (4), we obtain the 1D coherent 3-wave inertial model of SBS by coupling the three Eqs. (1, 2, & 6).

#### 4.2. Dynamical regimes

Implementing numerically this inertial model with parameters corresponding to various experimental devices, either in ring [6, 10] or in line [17] geometries, and various values of  $\alpha$ , we were not able to obtain asymptotically stable solitonic regimes. This result holds both for initial conditions starting from an uniform noise, and when the acoustic dispersion (i.e. Eq. (6)) is 'switched on' from an initial condition corresponding to a fully stable solitonic regime obtained with the dispersionless model (Eqs (1,2 &3) with otherwise identical parameters.

Indeed, when a significant positive acoustic dispersion  $\alpha > 0.1$  was taken into account, all simulated devices asymptotically evolved towards a quasi-cw SBS mirror regime, either after a only few roundtrip times in the former case (noisy initial condition), or after very long transitories in the latter (solitonic initial condition).

#### 4.3. Novel SBS mirror regime with inverted acoustic profile

For long enough evolution times (typically, several hundred roundtrip times, starting from a pulsed initial condition), all configurations yield stationary regimes for the intensities of the three waves. The three phases may continue to evolve, as a fully stationary asymptotic regime was never reached even for very long simulation times.

An unexpected feature of this new inertial SBS mirror is that the spatial distribution of the acoustic wave is inverted. Indeed, while in the usual, dispersionless SBS mirror (§2.2), the amplitude of the acoustic wave monotonously decreases from its maximum value at the fiber end closest to the pump laser (Fig. 1), it now monotonously *increases* from the input end towards the far end of the fiber (upper part of Fig. 3) in this new inertial mirror regime.

Another remarkable feature is that this new mirror regime is obtained even for very low SBS gains of the order of  $G = 1$  or below ( $G = 0.05$  in Fig. 3), to be compared to the  $G = 14.5$  used in the common mirror of Fig. 1. This is a direct consequence of the build-up of a very strong acoustic wave at the far end of the fiber: the SBS dynamics and the efficiency of the SBS mirror is no longer determined either by the level of spontaneous acoustic noise [2] or by the reinjected Brillouin intensity [9], but by the intensity of the acoustic wave.

As can be seen on the lower part of Fig. 3, while the spatial profile of the intensities have reached a stable enough asymptotic regime by  $t = 341$  roundtrip times, this is not entirely true for the phases, which still continue to slowly evolve.

For higher values of the dispersion the inverted mirror presents an almost total reflection, thus a reflectivity  $\sim 1$  as is shown in the upper part of Fig. 4 ( $\alpha = 0.5, G = 0.35$ ) and Fig. 5 ( $\alpha = 0.55, G = 0.55$ ). On the other hand, a more complex and rapid phase dynamics sets up at the far end of the fiber, while the amplitude of the acoustic wave (and thus the acoustic pressure) is already one order of magnitude higher at the far end of the fiber than in the previous case (lower part of Figs. 4 & 5).

It is interesting to note that this fast phase dynamics, which can be interpreted in terms of a significant spectral broadening of the two optical waves, remains localized near the far end of the fiber, with a rather slow variation of the phases on the pump laser side, meaning a still very coherent Brillouin output. The dynamical self-correction of this complex phase dynamics upstream of the phase-turbulent zone is reminiscent of the dynamic self-stabilization process of ultra-coherent SBS lasers [6].

For even higher values of the acoustic dispersion ( $\alpha = 1$ ), the same process are observed, only faster (with the inverted mirror fully established in only about 400 roundtrip times, to be compared to the 1000 of the previous case), and with a far more efficient accumulation process of the acoustic wave, yielding potentially huge values of the acoustic intensity, to the point of

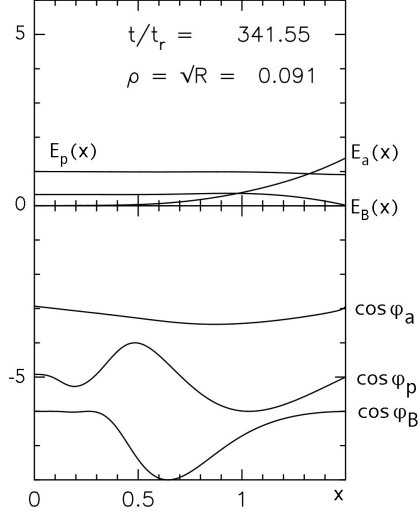


Fig. 3. SBS mirror with an inverted acoustic profile for a moderate acoustic dispersion ( $\alpha = 0.11$ ) and a very low gain ( $G = 0.05$ ): Spatial distribution of the amplitudes and phases of the three waves (pump, Brillouin, acoustic) (numerical, dimensionless abscissa  $x/\Lambda$  with  $L/\Lambda = 1.49, \mu = 59.96, \sqrt{R} = 0.091$ ). The very strong damping avoids total mirror reflection. Note the *increasing* acoustic intensity at the far end of the fiber (top right).

mechanically damaging the fiber [57].

#### 4.4. Discussion

Conventional wisdom suggests that an usual SBS mirror is established when the gain is sufficient for the three waves to reach together a sufficient intensity, which normally happens near the laser input end of the device, where the pump intensity is maximal, having not been depleted yet, as well as the Brillouin intensity, after a cumulative amplification process during its propagation along the fiber, the much smaller acoustic intensity being mostly considered as a slave variable in the stationary approximation. Eq. (3) then yields  $E_a = \frac{K_{SBS}}{\gamma_a} E_p E_B^*$  if the acoustic propagation term is neglected, thus  $\varphi_a = \varphi_p - \varphi_B$  and  $\Phi \sim 0$ , that is, a permanent reconstruction of the acoustic wave through a succession of Stokes ( $\Phi < \pi$ ) and antiStokes ( $\pi < \Phi < 2\pi$ ) SBS sequences, and a reduced efficiency of the usual Brillouin mirror whenever the relative phases of the three waves evolve rapidly, whether due to the low coherence of the pump or here, to the propagation properties of the acoustic wave in presence of strong acoustic GVD.

A direct corollary is that the phase of the acoustic wave 'mirrors' the fluctuations of the pump wave to maintain not only  $\Phi \sim 0$ , but also a fairly constant phase  $\varphi_B = \varphi_p - \varphi_a - \Phi$  for the Brillouin wave [6] accounting for the nonlinearly self-stabilized ultracoherent SBS laser regimes [5, 6, 8].

Let us now consider the opposite situation, when the *pump* is the weakest of the three waves. Conversely, this is most likely to happen at the far end of the device, where the pump wave is mostly depleted, while a significant Brillouin amplitude has just been fed through the cavity

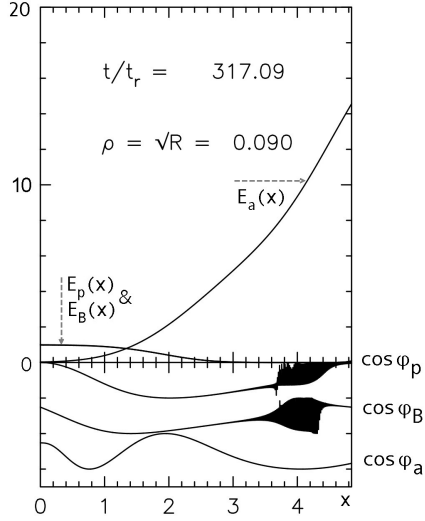


Fig. 4. SBS mirror with an inverted acoustic profile for an acoustic dispersion  $\alpha = 0.5$  showing total reflection. (numerical, dimensionless abscissa  $x/\Lambda$  with  $L/\Lambda = 3.86, G = 0.35, \mu = 22.07, \sqrt{R} = 0.09$ ). Asymptotic stage for the intensities.

feedback. It is no longer the acoustic wave, but the pump wave itself that will act as an 'absorber' of the rapid phase evolution of the other two waves to maintain  $\Phi \sim 0$  and an efficient SBS process. Note that since, to the first order,  $\partial_t \varphi_i \propto 1/E_i$  [42], the closer to the input end of the fiber and the higher the pump amplitude, the less efficient this mechanism.

The above-mentioned phase self-stabilization process now operates to the benefit of the *acoustic* wave, with the phase of the pump wave mirroring the fluctuations of the phase of the Brillouin wave to maintain  $\Phi \sim 0$ , and a fairly constant phase  $\varphi_a = \varphi_p - \varphi_B - \Phi$ , yielding an ultracoherent acoustic wave inside the fiber. Fig. 6 presents two levels of zooming on the phase dynamics in the right-hand part of Fig. 5 (namely, near  $x = 4$ ). Note, on the left-hand part of Fig. 6, the small but significant acoustic phase gradient, which constitutes a signature of a very coherent but slightly off-resonance acoustic wave, and on its right-hand part, at a stronger magnification rate, the slight spatial shift between the strongly (anti-)correlated, yet distinct phase patterns of the two optical waves. A direct corollary is the possibility of locally very narrow acoustic spectra, potentially yielding linewidths in the Hz range or below. [5]

Another key difference between the two situations is that while, taking into account the very low quality factor of the cavity, the average Brillouin intensity cannot significantly exceed the input pump intensity  $I_p^0$ , the same limitation does not apply to the acoustic wave (or rather, would only apply for values of  $I_a^L$  of the order of  $\frac{c}{c_a} I_p^0 \sim 10^5 I_p^0$ ). For the acoustic wave, the finite amplification length is the limiting factor.

Finally, we note that, somewhat counter-intuitively, a strong acoustic dispersion may increase the efficiency of SBS amplifiers, since the inverted SBS mirror regime appears very effective, with reflection rates close to 100% for relatively low gain values, such as  $G = 0.35$ .

Due to numerical stability problems of our 4-point Runge-Kutta algorithm, we were not able

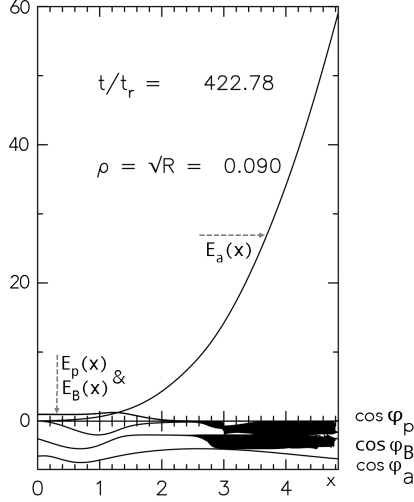


Fig. 5. SBS mirror with an inverted acoustic profile for a strong acoustic dispersion  $\alpha = 1.0$  showing total reflection and turbulent pump and Brillouin phases at the far end of the fiber (right). Asymptotic stage (numerical,  $G = 0.55, L/\Lambda = 4.84, \mu = 17.60, \sqrt{R} = 0.09, t/t_r = 422.78$ ).

to reliably implement this inertial model with perturbative values of the acoustic dispersion, but only for values of  $\alpha > 0.1$ . Thus, we couldn't obtain in this frame the usual SBS mirror regimes, as observed with the 3-wave model with perturbative acoustic dispersion, nor explore numerically the transition towards the inverted SBS mirror regime for increasing values of the pump power (thus of  $\alpha$ ).

However, formal calculations (see Appendix) allowed us to plot the temporal growth rate  $\gamma$  [not to be confused with the loss coefficients  $\gamma_e$  and  $\gamma_a$ ] of an acoustic perturbation as a function of  $\alpha$ . A key result is that any such perturbation is initially unstable ( $\gamma > 0$ ) for any positive value of the acoustic dispersion,  $\alpha > 0$ , and even for some negative values (Fig. 7). The inertial regime may thus yield a full mirror behavior even for relatively small values of the acoustic dispersion.

## 5. Identification of regions of strong inertial dispersion

To identify the spectral regions of strong acoustic dispersion in which we may expect to observe the new inverted SBS mirror regime, as well as, conversely, the regions of weak dispersion where a bridge could be established between the two models, inertial and perturbative, we shall search the maximum values of the temporal growth rate of the acoustic amplitude,  $\gamma$ , that is, the *extrema* of the function  $\gamma(k, \alpha)$ .

To this end, and for the simplicity of the already bulky expressions, we will from now on shift to reduced variables, defining the reduced acoustic amplitude  $A_a = E_a/|E_p^0|$ , the reduced acoustical losses  $\mu = \gamma_a/K_{SBS}|E_p^0|$ , and setting:

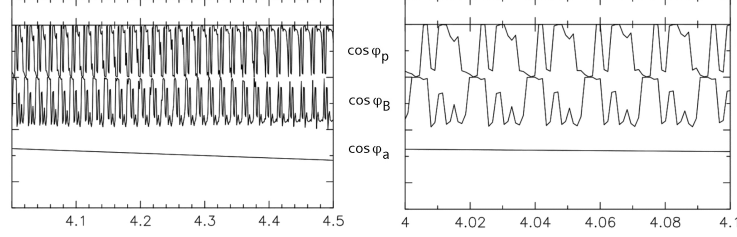


Fig. 6. Same as Fig. 5: Successive zooms on the spatial evolution of the phases. Note the strong anticorrelation of the phases of the pump and Brillouin waves, yielding an almost uniform phase of the acoustic wave ( $\Phi = \phi_p - \phi_B - \phi_a \sim Cst$ )

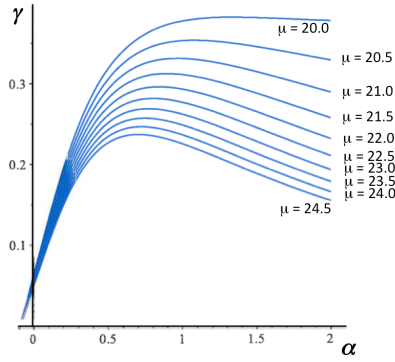


Fig. 7. Temporal acoustic growth rate  $\gamma$  as a function of the acoustic dispersion  $\alpha$  for a set of values of the dissipation from  $\mu = 20$  to  $\mu = 24.5$ , as obtained from the dispersion equation. Note that  $\gamma > 0$  for any  $\alpha > 0$ .

$$t/\tau = tK_{SBS}|E_p^0| \rightarrow t \quad x/\Lambda_0 = xnK_{SBS}|E_p^0|/c \rightarrow x \quad (7)$$

The linearized complex evolution equation for the acoustic amplitude now reads:

$$[\partial_t + \varepsilon\partial_x + \mu + i\alpha(\partial_{tt} + 2\mu)] (\partial_t + \partial_x)A_a = A_a \quad (8)$$

Let us take:

$$\partial_t \rightarrow \gamma + i\omega \quad \partial_x \rightarrow ik \quad (9)$$

in order to obtain the complex characteristic equation:

$$[\gamma + i\omega + i\varepsilon k + \mu + i\alpha(\gamma^2 + 2i\omega\gamma - \omega^2 + 2\mu)] (\gamma + i\omega + ik) = 1 \quad (10)$$

giving rise to two real equations for the variables  $\gamma$ ,  $\omega$ ,  $k$  and  $\alpha$ :

$$\gamma^2 - \omega^2 + \mu\gamma - \omega k - \varepsilon\omega k - \alpha\gamma^2\omega + \alpha\omega^3 - \alpha\gamma^2k - 2\alpha\mu\omega - 2\alpha\mu k - \varepsilon k^2 - 2\alpha\omega\gamma^2 + \varepsilon\gamma k = 1 \quad (11)$$

$$2\omega\gamma + \gamma k + \varepsilon k\gamma + \mu\omega + \mu k + \alpha\gamma^3 - 3\alpha\omega^2\gamma + 2\alpha\mu\gamma - 2\alpha\omega\gamma k = 0 \quad (12)$$

The aim is to eliminate  $\omega$  from both equations to obtain an equation  $\gamma = \gamma(k, \alpha)$  and calculate  $Max[\gamma(k, \alpha)]$  with respect to the parameter  $\alpha$ . Ordering both equations in polynomial form with respect to  $\omega$ , we get:

$$\alpha\omega^3 - \omega^2 - (k + \varepsilon k + 3\alpha\gamma^2 + 2\alpha\mu)\omega + \mu\gamma - \alpha\gamma^2k - 2\alpha\mu k - \varepsilon k^2 + \varepsilon\gamma k + \gamma^2 = 1 \quad (13)$$

$$- (3\alpha\gamma)\omega^2 + (2\gamma + \mu - 2\alpha\gamma k)\omega + \gamma k + \varepsilon\gamma k + \mu k + \alpha\gamma^3 + 2\alpha\mu\gamma = 0 \quad (14)$$

These cubic Eq. (13) and quadratic Eq. (14) equations in  $\omega$  can be solved, but the elimination of  $\omega$  leads to a lengthy polynomial expression for  $\gamma = \gamma(k, \alpha)$  (detailed in the Appendix: Eq. (15)), which maximum with respect to  $\alpha$  can only be found numerically. Formal calculations using the Maple algorithm confirm that certain values of the acoustic (thus of the pump) frequency maximize the acoustic dispersion up to values where it can be considered strong.

Working Eq.(15) with Maple also allowed us to look into the dependence of the reduced dispersion  $\alpha$  over the wavevector  $k$ . For a given value  $\mu$  of the losses, we obtain a double implicit mathematical solutions  $\alpha(k)$  of Eq. (15), as shown in Figure 8. Of these two, only the lower one presents a physical meaning. The apparent avoided crossing between the upper and the lower solutions defines a critical value of the wavevector,  $k^{crit}$ , below which the dispersion reaches very high values (almost vertical section in Fig. 8, yielding  $k^{crit} \sim 2.8$  for  $\mu = 21$ ).

Moreover, since  $\omega$  varies almost linearly with  $k$  (Fig.9), we can also deduce a critical acoustic frequency  $\omega_a^{crit}$  below which the dispersion may be strongly enhanced.

## 6. Conclusion

We have established that, for singular values of the pump wavelength associated to high values of the acoustic group velocity dispersion, which may be observed in photonic crystal fibers, this latter parameter can have a significant influence on the dynamics of SBS devices.

We have further established the possibility of a new SBS mirror regime with an inverted spatial acoustic profile, which may offer a high reflectance ( $\sim 100\%$ ) even for rather small pump intensities for some special frequencies at which the acoustic dispersion is strong enough, that may appear with a high spectral selectivity in PCFs of, possibly, in specially designed Brillouin microcavities.

We have also identified a new nonlinear self-stabilisation process of the phase of the acoustic wave, which may occur in the inverted mirror regime when the pump intensity is severely depleted and drops to very low values.

Further research will nevertheless be needed in order to validate the full 3-wave inertial model of stimulated Brillouin scattering for weak or moderate values of the acoustic dispersion and/or of the pump power and determine the respective validity domains of this inertial model and of the perturbative acoustic dispersion model.

## Disclosures

The authors declare no conflict of interest.

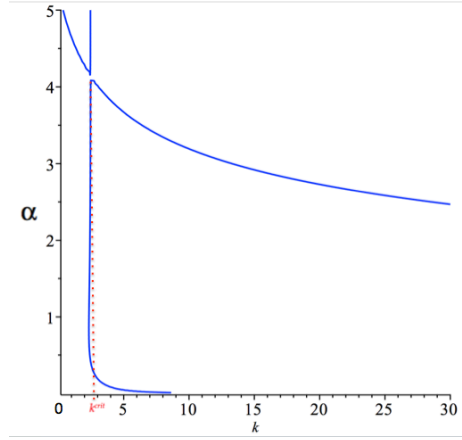


Fig. 8. Implicit solutions  $\alpha(k)$  of the dispersion relation (Eq. 15) for  $\gamma = 0.35$ ,  $\varepsilon = 10^{-5}$  and  $\mu = 21$ . Note, on the upper left, the avoided crossing between the upper and lower solutions, only the latter having a physical meaning, and the almost vertical slope below  $k^{crit} \sim 2.8$ .

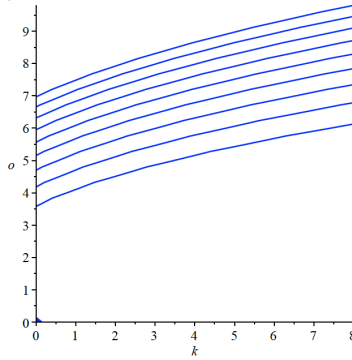


Fig. 9. Quasi-linear dispersion relation  $\omega(k)$  for  $\gamma = 0.2573$ ,  $\alpha = 0.745$ ,  $\varepsilon = 0$  and a set of values of the dissipation from  $\mu = 4$  to  $\mu = 20$ , allowing to deduce  $\omega^{crit}$  from  $k^{crit}$ .

## 7. Appendix: Resolution of the complex dispersion relation in the inertial limit

Eqs. (13) and (14) contain six variables, namely  $\omega$ ,  $k$ ,  $\varepsilon = \frac{ca}{c}$ , the reduced acoustic dispersion  $\alpha$  and losses  $\mu$ , and the growth rate  $\gamma$  of the acoustic instability.

We are interested on the function  $\gamma(\alpha)$  and we thus keep the other variables as known parameters. Eliminating  $\omega$  and calculating the lexicographical Gröbner basis expression [58], we

obtain the following 5-parameter polynomial :

$$\begin{aligned}
E = & 64\gamma^9\alpha^4 - 3\gamma^7\alpha^4k^2 - 8\gamma^5\alpha^4k^4 + 192\gamma^7\mu\alpha^4 + 96\gamma^7\varepsilon\alpha^3k + 18\gamma^6\varepsilon\alpha^3k^2 - 68\gamma^5\mu\alpha^4k^2 \\
& - 34\gamma^5\varepsilon\alpha^3k^3 + 8\gamma^4\varepsilon\alpha^3k^4 - 16\gamma^3\mu\alpha^4k^4 - 8\gamma^3\varepsilon\alpha^3k^5 + 144\gamma^5\mu^2\alpha^4 + 64\gamma^7\alpha^3k \\
& + 60\gamma^6\mu\alpha^3k + 144\gamma^5\mu\varepsilon\alpha^3k + 9\gamma^5\varepsilon^2\alpha^2k^2 + 108\gamma^4\mu\varepsilon\alpha^3k^2 - 124\gamma^3\mu^2\alpha^4k^2 \\
& + 54\gamma^4\varepsilon^2\alpha^2k^3 + 4\gamma^5\alpha^3k^3 - 10\gamma^4\mu\alpha^3k^3 - 124\gamma^3\mu\varepsilon\alpha^3k^3 - 31\gamma^3\varepsilon^2\alpha^2k^4 + 32\gamma^3\mu^3\alpha^4 \\
& - 36\gamma^5\mu\varepsilon\alpha^2k + 116\gamma^5\mu\alpha^3k + 128\gamma^4\mu^2\alpha^3k + 48\gamma^3\mu^2\varepsilon\alpha^3k + 58\gamma^5\varepsilon\alpha^2k^2 \\
& + 64\gamma^4\mu\varepsilon\alpha^2k^2 + 24\gamma^3\mu\varepsilon^2\alpha^2k^2 + 4\gamma^3\varepsilon^3\alpha k^3 - 12\gamma^4\varepsilon\alpha^2k^3 + 6\gamma^3\mu\varepsilon\alpha^2k^3 \\
& + 8\gamma^3\mu\alpha^3k^3 - 20\gamma^2\mu^2\alpha^3k^3 + 4\gamma^3\varepsilon\alpha^2k^4 - 10\gamma^2\mu\varepsilon\alpha^2k^4 + 32\gamma^7\alpha^2 + 16\gamma^6\mu\alpha^2 \\
& - 12\gamma^5\mu^2\alpha^2 + 36\gamma^4\mu\varepsilon\alpha^2k - 18\gamma^5\alpha^3k - 24\gamma^3\mu^2\alpha^3k + 16\gamma^2\mu^3\alpha^3k + 18\gamma^4\varepsilon^2\alpha k^2 \\
& + 10\gamma^5\alpha^2k^2 + 12\gamma^4\mu\alpha^2k^2 + 6\gamma^3\mu^2\alpha^2k^2 - 24\gamma^3\mu\varepsilon\alpha^2k^2 + 16\gamma^2\mu^2\varepsilon\alpha^2k^2 - 6\gamma^3\varepsilon^2\alpha k^3 \\
& + 4\gamma^2\mu\varepsilon^2\alpha k^3 - 8\gamma^3\alpha^3k^3 - 4\gamma^3\alpha^2k^4 - 4\gamma^2\mu\alpha^2k^4 + 48\gamma^5\mu\alpha^2 + 32\gamma^4\mu^2\alpha^2 - 8\gamma^3\mu^3\alpha^2 \\
& + 24\gamma^5\varepsilon\alpha k + 16\gamma^4\mu\varepsilon\alpha k - 4\gamma^3\mu^2\varepsilon\alpha k + 54\gamma^4\varepsilon\alpha^2k - 108\gamma^3\mu\alpha^3k + 18\gamma^4\varepsilon\alpha k^2 \\
& + 12\gamma^3\mu\varepsilon\alpha k^2 - 3\gamma^2\mu^2\varepsilon\alpha k^2 - 12\gamma^3\mu\alpha^2k^2 - 12\gamma^2\mu^2\alpha^2k^2 + 8\gamma\mu^3\alpha^2k^2 - 54\gamma^3\varepsilon\alpha^2k^2 \\
& - 6\gamma^3\varepsilon\alpha k^3 - 6\gamma^2\mu\varepsilon\alpha k^3 + 4\gamma\mu^2\varepsilon\alpha k^3 + 36\gamma^4\mu\alpha^2 + 4\gamma^3\mu^2\alpha^2 - 4\gamma\mu^4\alpha^2 + 20\gamma^5\alpha k \\
& + 32\gamma^4\mu\alpha k + 7\gamma^3\mu^2\alpha k - 5\gamma^2\mu^3\alpha k + 4\gamma^3\mu\varepsilon\alpha k - 4\gamma\mu^3\varepsilon\alpha k + \gamma^3\varepsilon^2k^2 - \gamma\mu^2\varepsilon^2k^2 \\
& + 12\gamma^3\alpha^2k^2 - 6\gamma^2\mu\alpha^2k^2 + 4\gamma^3\alpha k^3 + 2\gamma^2\mu\alpha k^3 - \gamma\mu^2\alpha k^3 + \mu^3\alpha k^3 - 36\gamma^3\mu\alpha^2 \\
& + 4\gamma^4\varepsilon k - 3\gamma^2\mu^2\varepsilon k - \gamma\mu^3\varepsilon k - 4\gamma^3\mu\alpha k + 4\gamma\mu^3\alpha k - 18\gamma^3\varepsilon\alpha k - 2\gamma^3\varepsilon k^2 + 2\gamma\mu^2\varepsilon k^2 \\
& + 4\gamma^5 + 4\gamma^4\mu - 3\gamma^3\mu^2 - 4\gamma^2\mu^3 - \gamma\mu^4 - 27\gamma^3\alpha^2 - 18\gamma^3\alpha k - 12\gamma^2\mu\alpha k + 3\gamma\mu^2\alpha k \\
& + \gamma^3k^2 - \gamma\mu^2k^2 - 4\gamma^3 + 3\gamma\mu^2 + \mu^3
\end{aligned} \tag{15}$$

From there, formal calculations in Maple allowed us to determine the growth rate  $\gamma$  as a function of  $\alpha$  for any given set of values of the other parameters (Fig. 7). These results appear mostly insensitive to the order of magnitude of the small parameter  $\varepsilon$ , from  $10^{-5}$  to about 0.1.

It also allowed to plot the acoustic dispersion  $\frac{d^2k}{d\omega^2}$  as a function of  $\omega_a$  (Fig. 10) (Note that this physical parameter may vary with  $\omega_a$  and  $I_p^0$  even as the reduced parameter  $\alpha = c_a \frac{d^2k}{d\omega^2} K_{SBS} \sqrt{I_p^0} / 2\omega_a$  remains constant.)

Figure 11 shows two sets of the same implicit mathematical solutions for different values of  $\mu$ . Note that these are not monotonous, almost parallel curves, as might appear at first glance, but two upper and two lower sets of solutions with avoided crossings, as emphasized by the zoom of Fig. 7.

## References

1. J. Botineau, C. Leycuras, É. Picholle, and C. Montes, "Stabilization of a stimulated brillouin fiber ring laser by strong pump modulation," *J. Opt. Soc. Am. B* **6**, 300–312 (1989).
2. R. W. Boyd, K. Rzaewski, and P. Narum, "Noise initiation of stimulated brillouin scattering," *Phys. Rev. A* **42**, 5514 (1990).
3. C. Tang, "Saturation and spectral characteristics of the stokes emission in the stimulated brillouin process," *J. Appl. Phys.* **37**, 2945 (1966).
4. R. Enns and I. Batra, "Saturation and depletion in stimulated light scattering," *Phys. Lett.* **28A**, 591–592 (1968).
5. S. Smith, F. Zarinetchi, and S. Ezekiel, "Narrow-linewidth stimulated brillouin fiber laser and applications," *Opt. Lett.* **16**, 393–395 (1991).
6. É. Picholle, C. Montes, C. Leycuras, O. Legrand, and J. Botineau, "Observation of dissipative superluminescent solitons in a brillouin fiber ring laser," *Phys. Rev. Lett.* **66**, 1454–1457 (1991).

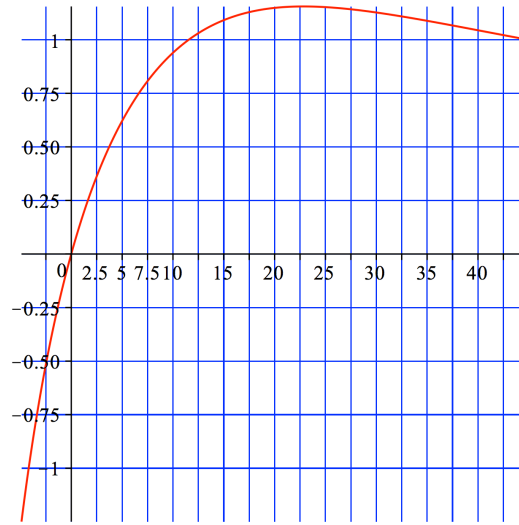


Fig. 10. Acoustic dispersion curve  $\frac{d^2k}{d\omega^2}(\omega)$  (numerical;  $\mu = 17.5$ ;  $\alpha = 0.8$ ;  $\gamma = 0.29$ ; and  $\varepsilon = 10^{-2}$ ). Note the strong maximum value of the dispersion ( $\frac{\beta_a^{dyn}}{c_a} > 1.55$ ) for  $\omega_a = 22.8$ .

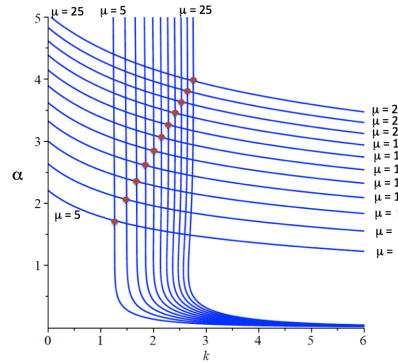


Fig. 11. Same as Fig. 7 for different values of the losses (left to right :  $\mu = 5$  to 25 by increments of 2). The dots figure the avoided crossings, visible on the zoomed Fig. 7 but not resolved at this scale. Only the lower part of the curves have a physical meaning.

7. H. H. Diamandi and A. Zadok, "Ultra-narrowband integrated brillouin laser," *Nat. Photonics* **13**, 9–10 (2018).
8. S. Gundavarapu, G. M. Brodник, M. Puckett, T. Huffman, D. Bose, R. Behunin, J. Wu, T. Qiu, C. Pinho, N. Chauhan, J. Nohava, P. T. Rakich, K. D. Nelson, M. Salit, and D. J. Blumenthal, "Sub-hertz fundamental linewidth photonic integrated brillouin laser," *Nat. Photonics* **13**, 60–67 (2019).
9. C. Montes, A. Mamhoud, and É. Picholle, "Bifurcation in a cw-pumped brillouin fiber ring laser: coherent sbs soliton morphogenesis," *Phys. Rev. A* **49**, 1344 (1994).
10. C. Montes, D. Bahloul, I. Bongrand, J. Botineau, G. Cheval, A. Mamhoud, É. Picholle, and A. Picozzi, "Self-pulsing and bistability in cw-pumped brillouin fiber ring laser," *J. Opt. Soc. Am. B* **16**, 932–951 (1999).
11. D. J. Kaup, "The first-order perturbed stimulated brillouin scattering equations," *J. Nonlinear Sci.* **3**, 1427 (1993).
12. A. L. Gaeta and R. W. Boyd, "Stochastic dynamics of stimulated brillouin scattering in an optical fiber," *Phys. Rev. A* **44**, 3205–3209 (1991).
13. R. G. Harrison, J. S. Uppal, A. Johnstone, and J. V. Moloney, "Evidence of chaotic stimulated brillouin scattering in optical fibers," *Phys. Rev. Lett.* **65**, 167 (1990).
14. S. Chen, F. Baronio, J. Soto-Crespo, P. Grelu, M. Conforti, and S. Wabnitz, "Optical rogue waves in parametric

- three-wave mixing and coherent stimulated scattering,” *Phys. Rev. A* **1992**, 033847 (2015).
15. D. Boukhaoui, D. Mallek, A. Kellou, H. Leblond, F. Sanchez, T. Godin, and A. Hiddeur, “Influence of higher-order stimulated brillouin scattering on the occurrence of extreme events in self-pulsing fiber lasers,” *Phys. Rev. A* **100**, 013809 (2019).
  16. B. J. Eggleton, C. G. Poulton, P. T. Rakich, M. J. Steel, and G. Bahl, “Brillouin integrated photonics,” *Nat. Photonics* **13**, 664–677 (2019).
  17. R. I. Woodward, E. Kelleher, S. Popov, and J. Taylor, “Stimulated brillouin scattering of visible light in small-core photonic crystal fibers,” *Opt. Lett.* **39**, 2330–2333 (2014).
  18. K. H. Tow, Y. Léguillon, S. Fresnel, P. Besnard, L. Brilland, D. Méchin, D. Trégoat, J. Trolles, and P. Toupin, “Linewidth-narrowing and intensity noise reduction of the second order stokes component of a low threshold brillouin laser made of  $ge_{10}as_{22}se_{68}$  chalcogenide fiber,” *Opt. Express* **20**, B104–B109 (2012).
  19. H. H. Diamandi, Y. London, A. Bergman, G. Bashan, J. Madrigal, D. Barrera, S. Sales, , and A. Zadok, “Opto-mechanical interactions in multi-more optical fibers and their applications,” *J. Sel. Top. Quantum Electron.* **26**, 2600113 (2020).
  20. J.-C. Beugnot, S. Lebrun, G. Pauliat, H. Maillotte, V. Laude, and T. Sylvestre, “Brillouin light scattering from surface acoustic waves in a subwavelength diameter optical fiber,” *Nat. Commun.* **5** (2014).
  21. A. Godet, A. Ndao, T. Sylvestre, V. Pecheur, S. Lebrun, G. Pauliat, J.-C. Beugnot, and K. P. Huy, “Brillouin spectroscopy of optical microfibers and nanofibers,” *Optica* **4**, 1232–1238 (2017).
  22. W. E. née Zhong, B. Stiller, D. Elser, B. Heim, C. Marquardt, and G. Leuchs, “Depolarized guided acoustic wave brillouin scattering in hollow-core photonic crystal fibers,” *Opt. Express* **23**, 27707–27714 (2015).
  23. F. Yang, F. Gyger, and L. Thévenaz, “Giant brillouin amplification in gas using hollow-core waveguides,” (2019). Preprint: arXiv:1911.04430v2.
  24. N. T. Otterstrom, R. O. Behunin, E. A. Kittlaus, Z. Wang, and P. T. Rakich, “A silicon brillouin laser,” *Science* **360**, 1113–1116 (2018).
  25. R. Dehghannasiri, A. A. Eftekhar, and A. Adibi, “Raman-like stimulated brillouin scattering in phononic-crystal-assisted silicon-nitride waveguides,” *Phys. Rev. A* **96**, 053836 (2017).
  26. F. Gyger, J. Liu, F. Yang, J. He, A. S. Raja, R. N. Wang, S. A. Bhave, T. J. Kippenberg, and L. Th’evenaz, “Observation of stimulated brillouin scattering in silicon nitride integrated waveguides,” *Phys. Rev. Lett.* **124**, 013902 (2020).
  27. J. Zhang, O. Ortiz, X. L. Roux, É. Cassan, L. Vivien, D. Marris-Morini, D. Lanzillotti-Kimura, and C. Alonso-Ramos, “Subwavelength engineering for brillouin gain optimization in silicon optomechanical waveguides,” *Opt. Lett.* **45**, 3717–3720 (2020).
  28. B. Morrison, A. Casas-Bedoya, G. Ren, K. Vu, Y. Liu, A. Zarifi, T. G. Nguyen, D.-Y. Choi, D. Marpaung, S. J. Madden, A. Mitchell, and B. J. Eggleton, “Compact brillouin devices through hybrid integration on silicon,” *Optica* **4**, 847–854 (2017).
  29. P. Dainese, P. S. J. Russell, G. S. Wiederhecker, N. Joly, H. L. Fragnito, V. Laude, and A. Khelif, “Raman-like light scattering from acoustic phonons in photonic crystal fiber,” *Opt. Express* **14**, 4141–4150 (2006).
  30. P. Dainese, P. S. J. Russell, N. Joly, J. Knight, G. S. Wiederhecker, H. L. Fragnito, V. Laude, and A. Khelif, “Stimulated brillouin scattering from multi-ghz guided acoustic phonons in nanostructured photonic crystal fibres guided acoustics,” *Nat. Phys.* **2**, 388–392 (2006).
  31. R. P. Moiseyenko and V. Laude, “Material loss influence on the complex band structure and group velocity in phononic crystals,” *Phys. Rev. B* **83**, 064301 (2011).
  32. J.-C. Beugnot and V. Laude, “Electrostriction and guidance of acoustic phonons in optical fibers,” *Phys. Rev. B* **86**, 224304 (2012).
  33. G. S. Wiederhecker, P. Dainese, and T. P. Mayer-Alegre, “Brillouin optomechanics in nanophotonic structures,” *APL Photonics* **4**, 0711101 (2019).
  34. G. Arregui, O. Ortiz, M. Esmann, C. M. Sotomayor-Torres, C. Gomez-Carbonell, O. Mauguin, B. Perrin, A. Lemaître, P. D. Garcia, and N. D. Lanzillotti-Kimura, “Coherent generation and detection of acoustic phonons in topological nanocavities,” *APL Photonics* **4**, 030805 (2019).
  35. G. P. Agrawal, *Nonlinear Fiber Optics* (Academic Press, 1989), 2nd ed.
  36. R. W. Boyd, *Nonlinear Optics* (Academic Press, 2008), 3rd ed.
  37. R. V. Laer, R. Baets, and D. V. Thourhout, “Unifying brillouin scattering and cavity optomechanics,” *Phys. Rev. A* **93**, 053828 (2016).
  38. C. Montes, “Efficient way to prevent reflection from stimulated brillouin backscattering,” *Phys. Rev. Lett.* **50**, 1129–1132 (1983).
  39. C. Montes, “Reflection limitation by driven stimulated brillouin rescattering and finite bandwidth spectral interaction,” *Phys. Rev. A* **31**, 2366–2374 (1985).
  40. J. Coste and C. Montes, “Asymptotic evolution of stimulated brillouin scattering: Implications for optical fibers,” *Phys. Rev. A* **34**, 3940–3949 (1986).
  41. C. Montes and J. Coste, “Optical turbulence in multiple stimulated brillouin backscattering,” *Laser Part. Beams* **5**, 405–411 (1987).
  42. J. Botineau, C. Leycuras, C. Montes, and É. Picholle, “A coherent approach to stationary stimulated brillouin fiber amplifiers,” *Annales des Télécommunications* **49**, 479–489 (1994).
  43. C. Wolff, M. J. Steel, B. J. Eggleton, and C. G. Poulton, “Stimulated brillouin scattering in integrated photonic

- waveguides: Forces, scattering mechanisms, and coupled-mode analysis,” *Phys. Rev. A* **92**, 013836 (2015).
44. V. Laude and J.-C. Beugnot, “Spontaneous brillouin scattering spectrum and coherent brillouin gain in optical fibers,” *Appl. Sci.* **8**, 907 (2018).
  45. É. Picholle and A. Picozzi, “Guided-acoustic-wave resonances in the dynamics of a brillouin fiber ring laser,” *Opt. Commun.* **135**, 327–330 (1997).
  46. I. Bongrand, É. Picholle, and A. Picozzi, “Coherent model of cladding brillouin scattering in single-mode optical fibers,” *Electron. Lett.* **34**, 1769 (1998).
  47. I. Bongrand, É. Picholle, and C. Montes, “Coupled longitudinal and transverse stimulated brillouin scattering in single-mode optical fibers,” *Eur. J. Phys. D* **20**, 121–127 (2002).
  48. R. Engelbrecht, “Analysis of sbs gain shaping and threshold increase by arbitrary strain distributions,” *J. Light. Technol.* **32**, 1689–1700 (2014).
  49. M. Maldovan, “Sound and heat revolutions in phononics,” *Nature* **503**, 209–217 (2013).
  50. S. A. Nikitov, R. S. Popov, I. V. Lisenkov, and C. K. Kim, “Elastic wave propagation in a microstructured acoustic fiber,” *IEEE transactions on ultrasonics, ferroelectrics, frequency control* **55**, 1831–1839 (2008).
  51. V. Laude, J. M. Escalante, and A. Martinez, “Effect of loss on the dispersion relation of photonic and phononic crystals,” *Phys. Rev. B* **88**, 224302 (2013).
  52. S. D. Lim, H. C. Park, K. Lee, and B. Y. Kim, “High-accuracy measurement of cladding noncircularity based on phase velocity difference between acoustic polarization modes,” *Opt. Express* **18**, 3574–3581 (2010).
  53. R. I. Woodward, É. Picholle, and C. Montes, “Brillouin solitons and enhanced mirror in the presence of acoustic dispersion in a small-core photonic crystal fiber,” in *Actes des 35<sup>e</sup> Journées Nationales d’Optique Guidée, Rennes, France*, (<https://hal.archives-ouvertes.fr/hal-01323737>, 2015).
  54. E. M. Dianov, A. Luchnikov, A. N. Pilipetskii, and A. Starodumov, “Electrostriction mechanism of soliton interaction in optical fibers,” *Opt. Lett.* **15**, 314–316 (1990).
  55. J. K. Jang, M. Erkintalo, S. G. Murdoch, and S. Coen, “Untraweak long-range interactions of solitons over galactical distances,” *Nat. Photonics* **7**, 657–663 (2013).
  56. C. Montes and A. Rubenchik, “Stimulated brillouin scattering from trains of solitons in optical fibers: information degradation,” *J. Opt. Soc. Am. B* **9**, 1857–1875 (1992).
  57. C. Montes and R. Pellat, “Inertial response to nonstationary stimulated brillouin backscattering: Damage of optical and plasma fibers,” *Phys. Rev. A* **36**, 2976–2979 (1987).
  58. D. A. Cox, J. Little, and D. O’Shea, *Ideals, Varieties and Algorithms* (Springer, 1992).